Engineering Science and Technology, an International Journal 22 (2019) 33–46

HOSTED BY

Contents lists available at ScienceDirect

Engineering Science and Technology, an International Journal

journal homepage: www.elsevier.com/locate/jestch

Full Length Article

Optimal distributed generation planning in distribution networks: A comparison of transmission network models with FACTS

A.A. Sadiq [a,*], S.S. Adamu [b], M. Buhari [b]

[a] Electrical and Electronics Engineering, Federal University of Techn., Minna, Nigeria
[b] Electrical Engineering, Bayero University, Kano, Nigeria

ARTICLE INFO

Article history:
Received 14 March 2018
Revised 12 September 2018
Accepted 29 September 2018
Available online 11 October 2018

Keywords:
Distributed Generator
FACTS
Transmission model
Distribution network
Thevenin's equivalent

ABSTRACT

In Distributed Generators (DG) optimal planning solutions, transmission section is modelled as an ideal voltage-controlled bus at 1.0 pu., this ignores the impacts of Flexible Alternating Current Transmission Systems (FACTS). However, modern transmission networks include optimally placed FACTS for improved power quality. Moreover, voltages at Point of Common Coupling (PCC) between transmission and distribution networks varies with FACTS control operations. Hence, these can result in local optimal DG planning solutions. In this paper, a two-bus Thevenin's equivalent model of transmission section to account for FACTS is proposed. Hybrid line voltage stability indices and particle swarm optimization (LVSI-PSO) obtain a reduced search space, location and sizes of FACTS at transmission section, while Particle Swarm Optimization (PSO) is used to locate and size DG in the distribution section of the test system. The test system is an integrated transmission-distribution network; with modified IEEE 9 bus as transmission section and IEEE 16 node as distribution section. Modification of driving point and transfer impedance of Z_{bus} matrix account for Thyristor Controlled Series Compensator (TCSC) and Static Var Compensator (SVC). Results show that solutions obtained with transmission network modelled as an ideal voltage-controlled bus is a local optimal solution compared with integrated transmission-distribution network model and Thevenin's equivalent model. The Proposed Thevenin's equivalent model through parameter estimations E_{th} and Z_{th} closely matches results from the integrated test system.

1. Introduction

Power utility companies of developing economies are embracing market driven/deregulated framework of power supply; replacing a proportion of conventional controlled grid structure. Features of deregulation includes: small capacities, renewable sources of generations, connected to distribution networks called DG. DGs possess technical abilities to improve power balance amidst demand and supply. Accordingly, behaviour of modern power systems is influenced by increased DG penetration due to support schemes for renewable energy, competitions and flexibilities in power systems operations [1–4].These results in operations of power systems with DGs in grid connected, micro grid and Islanded operations [5,6]. Hence, existing power grid infrastructures are going to be operated closer to their limits with resulting effect on the entire power system network [7–9]. This transition presents some challenges in power system's planning and operations. The challenges are associated either with technological or structural changes such as issues of optimal location and sizes of DG units [10].

One of the key challenges of deregulated framework of power supply is optimal planning (location and sizes) of DG units for networks [11,12]. In optimal DG planning in Distribution Network (DN), often the upper section (Generation and Transmission components) of the power system is assumed solidly stable, modelled as 1.0 p.u and represented as the reference or slack bus.

Although ideal voltage source representation of transmission systems is often reasonably adopted by researchers to reduce the complexity of optimisation problem-solving, this assumption is associated with inadequate modelling of impacts of FACTS and transmission equipment on optimal DG planning in DN [13]. The impacts coupled with loading level can worsen distribution section's power quality indices in terms of power losses, voltage stability and deviations as well as DG optimal planning solution [14]. This paper investigates impacts of transmission network models with FACTS on optimal location and sizes of DG in a multi-feeder DN (IEEE 16 node) and a typical comparison to the model of same network reported in [15].

* Corresponding author.
E-mail address: ahmad.abubakar@futminna.edu.ng (A.A. Sadiq).
Peer review under responsibility of Karabuk University.

https://doi.org/10.1016/j.jestch.2018.09.013
2215-0986/

Nomenclature

Nomenclature

B_{cap}	SVC capacitive susceptance
B_{ind}	SVC inductive susceptance
B_{sh}	bus shunt susceptance
B_{svc}	SVC susceptance
B_{total}	total bus susceptance
E_{th}	Thevenin's equivalent voltage
J_1	power loss term
J_2	voltage deviation term
J_3	voltage stability index term
K	number of terms in fitness function
$LCPI$	line collapse Proximity Index
LQP	line stability factor
L_m	type of line voltage index
L_{ij}	fast voltage stability index
L_{mn}	line stability index
PQ_{load}	net active and reactive load of distribution section
P_G^i	active power generation at node/bus i
P_L^i	active load at node/bus i
P^{loss}	active power loss without FATCS and DG
$P_{DG-facts}^{loss}$	active power loss with FATCS and DG
P_r	line receiving end active flow
P_s	line sending end active flow
P_{DG}	active power injection by DG
P_{DN}	net distribution section active load
$P_{injected}$	active power injection
P_{li}	active load at node i
P_{nli}	active load at node i with DG
Q_G^i	reactive power generation at node/bus i
Q_L^i	reactive load at node/bus i
Q_{svc}^{max}	maximum Var injection by SVC
Q_{svc}^{min}	minimum Var injection by SVC
Q_r	line receiving end reactive flow
Q_{DG}	reactive power injection by DG
Q_{DN}	net distribution section reactive load
$Q_{injected}$	reactive power injection
Q_{li}	reactive load at node i
Q_{nli}	reactive load at node i with DG
Q_{svc}	Var injection by SVC
R_{th}	real part of thevenin's impedance
V^{idx}	line voltage index without FATCS and DG
$V_{DG-facts}^{idx}$	voltage index with FATCS and DG
V_D	net voltage deviation
V_i	bus/node-i voltage magnitude
V_j	bus/node-j voltage magnitude
V_{pcc}	source voltage magnitude at PCC
X_{TCSC}	TCSC reactance
X_{TCSC}^{max}	upper limit of TCSC reactance
X_{TCSC}^{min}	lower limit of TCSC reactance
X_{line}	transmission line reactance
X_{th}	imaginary part of thevenin's impedance
Y_{DN}^L	constant admittance equivalent load
Z_{DN}^L	constant impedance equivalent load
Z_{bus}	system bus impedance matrix
Z_{pcc}	driving point impedance
Z_{th}	Thevenin's equivalent impedance
δ	bus/node voltage angle difference
δ_i	bus/node-i voltage angle
δ_j	bus/node-j voltage angle
δ_r	receiving bus/node voltage angle
δ_s	sending bus/node voltage angle
g_k	conductance of transmission line
nb	number of buses
nl	number of lines
r_i	rank of *i*th objective
r_{TCSC}	TCSC percentage compensation
Z	line impedance
R	line resistance
X	line reactance
Y_{ij}	magnitude of node admittance matrix
θ_{ij}	angle of node admittance matrix
θ	line impedance angle
V_s	line sending end voltage
i_{th}	node-numbered i
A	pie line model parameter A
B	pie line model parameter B
α	angle of pie line model parameter **A**
β	angle of pie line model parameter **B**
α_1	weight factor of J1
α_2	weight factor of J2
α_3	weight factor of J3

List of abbreviation

BER	Battery Energy Storage
DFIG	doubly fed induction generators
DG	Distributed Generators
DN	Distribution Network
FACTS	Flexible Alternating Current Transmission Systems
FVSI	Fast Voltage Stability Index
GCPV	grid-connected photovoltaic
HV/MV	high voltage or medium voltage
LVSI-PSO	hybrid line voltage stability indices and particle swarm optimization
MLDG	multiple location distributed generator
PCC	Point of Common Coupling
PQ	active and reactive loads
PSO	Particle Swarm Optimization
SPV	Solar Photovoltaic
SST	Solid State Transformer
SVC	Static Var Compensator
TCSC	Thyristor Controlled Series Compensator

1.1. Related work

In [1], impact of different degree of Grid-connected Photovoltaic (GCPV) DG penetration is investigated, DG size limited to 3 kW. Transmission network and associated equipment are represented with substation and modelled as single equivalent generator. The study neglected impacts of FACTS on GCPV sizes and uses fixed sizes. Impact of different DG operation mode on power quality of IEEE 123 node distribution feeder is reported by [3]. Direct repeated power flow with a step of 50 kVA is used to obtain DG sizes while PSO determines the locations of DG with minimization of total power loss as objective. Impacts of transmission network's parameter control were however ignored and discrete DG sizes were assumed. Similarly, optimal size and location of Solar Photovoltaic (SPV) based multiple location distributed generator (MLDG) in IEEE 33 and 69 distribution test systems was documented in [4]. The so called "2/3 rule" determines size and location of DG, the study assumes transmission network is solidly stable and represented by substation. Impact of large scale PV systems on voltage stability of IEEE 14 bus network was reported in [16]. Optimal node at which PV system is integrated is simply determined as the weakest node rather than aimed at a defined objective. Although

in [17], a recursive approach and ranked evolutionary particle swarm optimization for location and size was used; again impact of FACTS on power quality indices were ignored.

Recently, researchers and power utilities have shown substantial interest in optimal DG planning in DN. The various multi-objective formulation for DG planning can be classified into technical [18,19] and economical [20–22]. As voltage deviation and stability are important technical indices, it is often considered in DG planning. However, most works in the literature ignores impacts of High voltage or Medium voltage (HV/MV) support devices on optimal DG planning in DN. In [23–26], optimal DG, DG and Battery Energy Storage (BER) or DG and Solid State Transformer (SST) were studied to enhance voltage regulation and control. Although, impacts of ZIP, time varying and non-linear loads were examined, voltage support by FACTS location at HV/MV was left out. In [27], a coordination scheme for OLTC, capacitor banks and DG for voltage regulation was proposed, FACTS contribution to voltage support is equally left out.

Consequently, DG optimal planning solutions were demonstrated at distribution voltage levels with inadequate impacts of FACTS. This is evident when entire generation and transmission components are modelled as voltage-controlled bus at 1.0 pu. Often in power systems operations, complex voltage at PCC between transmission and distribution networks varies. The complex voltage changes with different operating point. These operating points may result from FACTS devices control operations at transmission side and/or type of DG models and amount of DG penetration at distribution side.

2. Proposed model of integrated transmission – distribution network

To account for FACTS in DG optimal planning in DN, a two-bus equivalent (Thevenin's equivalent) of transmission section to model an integrated transmission-distribution network is hereby proposed. The proposed approach aims at a realistic transmission section model to account for FACTS in DG planning compared to the model which assumes a slack bus at 1.0 pu. FACTS operations may cause voltage variation at PCC away from 1.0 pu. Thrust of proposed approach lies in variation of voltage vector at PCC between transmission and distribution networks, hence the Thevenin's model can account for voltage changes due to FACTS operations.

Transmission section of an integrated transmission-distribution network can be represented by two-bus equivalent shown in Fig. 1; where generator with voltage E_{th} transfers power through transmission line having an impedance of $Z_{th} = R_{th} + X_{th}$ into the distribution network at voltage V (PCC). Transmission section (with FACTS) is thus modelled with Thevenin's equivalent parameters E_{th} and Z_{th}.

2.1. Thevenin's model of transmission network with FACTS

Detail procedure for finding Thevenin's equivalent of power system involves use of power flow solutions and Z_{bus} matrix formulation [28]. Thevenin's voltage is obtained from power flow solution with all loads including net load at PCC; while Z_{bus} matrix formulation are obtained with all loads modelled as constant impedances. At this stage, net distribution section active and reactive load demand (net PCC load) is converted into an equivalent constant impedance. Thus, Thevenin's voltage and impedance of the transmission section excluding the distribution section is therefore obtained by nullifying the effect of distribution section [29]. Thevenin's parameters are obtained by Eqs. (1) and (2).

$$Z_{th} = \frac{Z_{pcc} * Z^L_{DN}}{Z^L_{DN} - Z_{pcc}} \tag{1}$$

$$E_{th} = \left(1 + \frac{Z_{th}}{Z^L_{DN}}\right) * V_{pcc} \tag{2}$$

In Eqs. (1) and (2), Z_{th} and E_{th} are Thevenin's impedance and voltage respectively. The Z_{pcc} is diagonal element of Z_{bus} matrix including net distribution section load and V_{pcc} is voltage magnitude at PCC from load flow.

The constant impedance equivalent of distribution section load Z^L_{DN}, is obtained using Eq. (3).

$$Z^L_{DN} = Y^L_{DN} = \frac{P_{DN} - Q_{DN}}{V^2_{pcc}} \tag{3}$$

where Y^L_{DN}, P_{DN} and Q_{DN} are equivalent admittance, net active and reactive load of the distribution section respectively.

Obtaining Thevenin's equivalent of the transmission section involves:

- *Load flow execution:* A load flow routine is executed to obtain the voltage at PCC.
- *Bus Impedance matrix formulation (Zbus):*
  - i. Convert all load of the transmission network into equivalent constant impedance using Eq. (3)
  - ii. Obtain driving point impedance of Z_{bus} corresponding to PCC bus.
- *Obtain Thevenin's equivalent:* E_{th} and Z_{th} are calculated using Eqs. (1) and (2)

Generally, a generator is modeled by internal voltage source E, behind a series reactance X to maintain a terminal voltage V. Although in load flow, since reactive output of PV generator is adjusted to maintain constant terminal voltage V (e.g.Fig. 1), generator is modelled by constant voltage source V neglecting series impedance.

2.2. Static model of TCSC in Thevenin's impedance

TCSC, a series compensator provides inductive or capacitive compensation [6]. Pie model of a transmission line with TCSC between bus-i and bus-j is shown in Fig. 2. TCSC is modelled as a variable impedance during steady state which modifies line impedance. To achieve power flow redistribution, TCSC increases or decreases effective impedance of transmission line. Therefore, to account for TCSC in Thevenin's impedance, modification of driving point and transfer impedance elements of the Z_{bus} matrix is

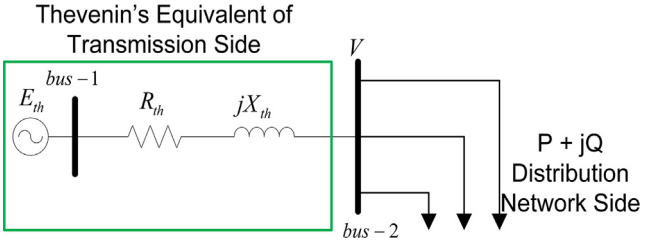

Fig. 1. Thevenin's equivalent of transmission network.

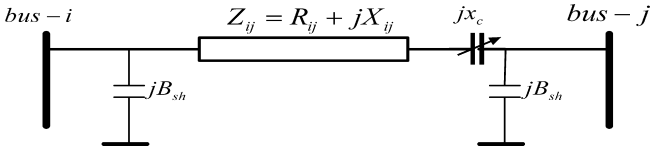

Fig. 2. Pie model of transmission line with TCSC.

obtained [30]. Alternatively, new line reactance with TCSC is given by Eq. (4).

$$X_{ij} = X_{line} + X_{TCSC} = r_{TCSC} * X_{line} \tag{4}$$

where X_{line} is reactance of transmission line, X_{TCSC} is reactance contributed by TCSC and r_{TCSC} is percentage compensation. TCSC reactance is often bounded between upper and lower limit; $X_{TCSC}^{min} \leqslant X_{TCSC} \leqslant X_{TCSC}^{min}$, which correspond to $-0.8 \leqslant X_{TCSC} \leqslant 0.2$ [31–34].

2.3. Static model of SVC in Thevenin's impedance

SVC is a shunt connected static Var generator or absorber, when SVC inject reactive power, it is capacitive and inductive as reactive power absorber. Fig. 3 shows the variable susceptance model of SVC with Var capacity within bounded limit. Driving point elements of the Z_{bus} matrix is modified to account for SVC susceptance B_{svc} in the Thevenin's equivalent. Alternatively, total shunt susceptance B_{total} at SVC bus is sum of B_{sh} and B_{svc} as given by Eq. (5) [35]. Reactive power Q_{svc} injected by SVC at bus-i to maintain voltage at V_i is given by Eq. (6).

$$B_{total} = B_{sh} + B_{svc} \tag{5}$$

$$Q_{svc} = V_i^2 * B_{svc} \tag{6}$$

Maximum and minimum reactive power output ($Q_{svc}^{max}, Q_{svc}^{min}$) of SVC can be set using inductive and capacitive susceptances B_{ind} and B_{cap} as given in Eqs. (7) and (8) respectively, SVC is bounded within -150 MVar $\leqslant Q_{svc} \leqslant$ 150 MVar [34,36].

$$Q_{svc}^{\max} = B_{ind} * V_i^2 \tag{7}$$

$$Q_{svc}^{\min} = B_{cap} * V_i^2 \tag{8}$$

3. DG model and modes of operation

Based on output terminal characteristics- ability to inject real and/or reactive power [36,37], DGs are often grouped into three major operating modes [2,12,38,39] namely:

(a) *PV-model:* DG which supplies only real power such as PV (Unity power factor models)
(b) *PQ-model:* DG which supplies real and reactive power (Constant power factor models).
(c) *Doubly fed induction generators (DFIG)-model:* DG which supplies real power but absorb/supplies reactive power.This study is aimed not on the dynamics and fast transients associated with power electronics interface DGs, rather on impacts of power injected by DG through optimal planning in distribution section to account for FACTS control operation. Consequently, DG can be modelled as negative active and reactive loads (PQ) [2]. If P_{li} and Q_{li} are real and reactive power consumed at the ith node of a distribution network, after DG is connected the new real and reactive power consumed (P_{nli}, Q_{nli}) is obtained as given in Eqs. (9) and (10).

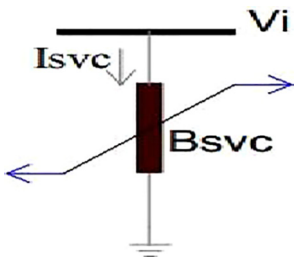

Fig. 3. SVC Connected at Bus-i.

$$P_{nli} = P_{li} - P_{DG} \tag{9}$$

$$Q_{nli} = Q_{li} - Q_{DG} \tag{10}$$

where P_{DG} and Q_{DG} are real and reactive power injections from DG.

Eqs. (9) and (10) are subject to real and reactive power balance given in Eqs. (11) and (12).

$$P_G^i - P_L^i - P_{injected}^i = 0 \tag{11}$$

$$Q_G^i - Q_L^i - Q_{injected}^i = 0 \tag{12}$$

where real and reactive power injected ($P_{injected}, Q_{injected}$) are computed as Eqs. (13) and (14) respectively.

$$P_{injected}^i = \sum_{j=1}^{n} V_i V_j Y_{ij} \sin(\delta_i - \delta_j + \theta_{ij}) \tag{13}$$

$$Q_{injected}^i = \sum_{j=1}^{n} V_i V_j Y_{ij} \cos(\delta_i - \delta_j + \theta_{ij}) \tag{14}$$

In Eqs. (11)–(14), P_G^i, Q_G^i, P_L^i, Q_L^i are active and reactive power generation and load respectively; complex voltages at nodes i and j are given by $V_i\angle\delta_i$ and $V_j\angle\delta_j$ while $Y_{ij}\angle\theta_{ij}$ is (i,j)th element of node admittance matrix.

4. Optimal placement of FACTS and DG

The Modified IEEE 9 bus transmission section is deficient in reactive power (Var), the effect is increased power loss and bus voltage below utility allowable limit of 0.9 pu. Therefore, the need for external compensation devices such as FACTS. TCSC and SVC are optimally placed and sized in Var deficient transmission section to reduced real power loss, improve voltage profile and static voltage stability using the proposed hybrid LVSI-PSO. Accordingly, with FACTS optimally placed and Thevenin's equivalent parameters obtained, determination of optimal location and size of DG is obtained using PSO. The problem's objective is formulated as a function (JJ) to minimizes three variables; J_1, J_2 and J_3 as stated in Eq. (15).

$$JJ = f(J_1, J_2, J_3) \tag{15}$$

subject to;

$$P_{DG-facts}^{loss} \leqslant P^{loss} \tag{16}$$

$$V_{DG-facts}^{idx} \leqslant V^{idx} \tag{17}$$

$$0.9 \leqslant V_i \leqslant 1.1 \tag{18}$$

where $P_{DG-facts}^{loss}, P_{loss}, V_{DG-facts}^{loss}$ and V_{idx}, are active losses, line voltage stability indices with/without DG-FACTS respectively.

4.1. Real power loss

Eq. (19) expresses real power loss of power system network mathematically [40]. The power loss term J_1 in (15) is normalized by its base value as expressed by Eq. (20).

$$P^{loss} = \sum_{k=1}^{nl} g_k (V_i^2 + V_j^2 - 2V_i V_j \cos(\delta_i - \delta_j)) \tag{19}$$

$$J_1 = \frac{P_{DG-facts}^{loss}}{P_{base}^{loss}} \tag{20}$$

where g_k is conductance of transmission line. V_i, V_j, δ_i, δ_j are the voltage magnitudes and angles at buses/nodes i and j respectively, nl is the number of lines in the network.

4.2. Voltage deviation

Net voltage deviation V_D away from ideal (1.0 pu.) is computed in Eq. (21). Voltage deviation term J_2 in Eq. (15) is also normalized by its base value and given in Eq. (22), where nb is the number of buses.

$$V_D = \sum_{i=1}^{nb} |1 - V_i| \tag{21}$$

$$J_2 = \frac{V_D}{V_{Dbase}} \tag{22}$$

4.3. Line voltage stability index

Several variants of line voltage stability indices were proposed in literatures [41]. At transmission section, four of such indices (L_{ij}, L_{mn}, L_{QP}, and $LCPI$) were evaluated to form reduce search space for LVSI-PSO, these indices are expressed in Eqs. (23)–(26).

$$L_{ij} = J_3 = \frac{4Z^2 Q_r X}{V_s^2 (R\sin\delta - X\cos\delta)^2} \tag{23}$$

$$L_{mn} = \frac{4XQ_r}{(V_s \sin(\theta - \delta)^2} \tag{24}$$

$$LQP = 4\left(\frac{X}{V_s^2}\right)\left(Q_r + \frac{P_s^2 X}{V_s^2}\right) \tag{25}$$

$$LCPI = \frac{4|\mathbf{A}|\cos\alpha(P_r|\mathbf{B}|\cos\beta + Q_r|\mathbf{B}|\sin\beta)}{(V_s\cos\delta)^2} \tag{26}$$

In Eqs. (23)–(26), Q_r, P_r and P_s are reactive and active power flow at receiving and sending end of a line respectively, V_s is sending end bus voltage. Z, R and X are line impedance, resistance and reactance respectively. θ is line impedance angle, $delta = delta_s - delta_r$, is voltage angular difference between the sending and receiving end buses. **A** and **B** are pie model parameters of transmission line while α and β are their respective phase angles [41].

In objective function of Eq. (15), line voltage stability index of Eq. (23) is adopted. A measure of voltage stability index of the network by L_{ij} is defined as sum of individual line stability indices as given in Eq. (27). Line voltage stability index term J_3 in (15) is also normalized by its base value and given in (28).

$$V^{idx} = \sum_{m\in nl} L_m \tag{27}$$

$$J_3 = \frac{V^{idx}_{DG-facts}}{V^{idx}_{base}} \tag{28}$$

Distribution networks are characterized by high reactance to resistance (x/r) ratio, to account for this in distribution section, L_m in Eq. (27) is the Fast Voltage Stability Index (FVSI) L_{ij} of Eq. (23) without assumptions (i.e. $\sin\delta \approx 0, \cos\delta \approx 1$) [41].

From Eq. (15), objective of DG placement is combined minimization of total power loss, voltage deviation and line voltage stability indices normalized by their respective base values. All PQ node of distribution section form DG location search space. Using Eqs. (19)–(23), the multi objective problem is therefore the minimization of a single fitness function given by Eq. (29).

$$Fitness = \alpha_1 * J_1 + \alpha_2 * J_2 + \alpha_3 * J_3 \tag{29}$$

where α_1, α_2 and α_3 are weight coefficients to measure contribution of each term to fitness function of Eq. (29).

At some value when the power injection from feeder located DG units exceed the power supplied from the transmission section, reverse power flow may cause voltage rise effects at PCC. To avoid voltage rise effects and reverse power flow, power utilities regulates the amount of power injection from various DG units [1,23,42–44]. Eq. (30) defines DG size operational constraints.

$$0 \leqslant DG_{size} \leqslant 0.75PQ_{load} \tag{30}$$

where, PQ_{load} is net active and reactive load of distribution section. Maximum power output by DG units is limited to 75% of PQ_{load}[42–44].

Therefore, the fitness expressed by Eq. (29) is subject to constraints of Eqs. (11), (12), (16)–(18). To assigned the weight factors of Eq. (29), rank sum of objective terms within direct weight elicitation technique is used [45] and given by Eq. (31).

$$\alpha_i = \frac{K - r_i + 1}{\sum_{j=1}^{K} K - r_j + 1} \tag{31}$$

where K and r_i are number of fitness function terms and rank of ith objective respectively. In ranking the objective terms, voltage deviation term J_2 is ranked third since voltage inequality constraint of Eq. (18) is imposed, while J_3 and J_1 are ranked second and first such that $\alpha_1 + \alpha_2 + \alpha_3 = 1$. As a result, the weights used are 0.5, 0.15 and 0.35 respectively.

5. Hybrid line voltage stability indices-particle swarm optimization (LVSI-PSO)

PSO is a swarm dependent optimization technique proposed by Kennedy and Eberhart (1995). Initially, a swarm is randomly generated to represent the solution, this makes solution dependent on initial swarm and can be prone to local optimal. To overcome this, PSO parameters (swarm size, maximum iteration, weighting factor and inertial weight) are carefully tuned [3,7]. However, the goal of LVSI-PSO is to obtain a reduce search space thereby avoiding local optimal solutions and improved performance. Based on LVSI values, search space is formed for optimal locations of FACTS. First few lines on LVSI ranking and buses common to these lines constitute reduce search space for TCSC and SVC locations respectively.

During swarm flight, particle's velocity and position updates is according to Eqs. (32) and (33) respectively.

$$V_i^{k+1} = \omega V_i^k + c_1 rand(Pbest_i^k - X_i^k) + c_2 rand(Gbest_i^k - X_i^k) \tag{32}$$

$$X_i^{k+1} = X_i^k + V_i^{k+1} \tag{33}$$

where, $V_i^{k+1}, V_i^k, X_i^{k+1}$ and X_i^k are the ith particle's velocity and position at $(k+1)$th and k_{th} iteration respectively. $P_{best}, G_{best}, C_1, C_2$, and ω are particle's personal best, global best, constant acceleration factors and inertia weight respectively.

A particle's position is modelled by a vector as expressed in Eq. (34), where λ and η are location and size respectively. To ensure particles remain within reduce search space, position update of LVSI-PSO is realised according to Eq. (35).

$$Position_i = [\lambda_i, \eta_i] \tag{34}$$

$$Postion_i(\lambda_i) = \begin{cases} X_i^{k+1}(\lambda_i) & if\ \lambda_i \in \mathbb{N} \\ X_i^k(\lambda_i) & if\ \lambda_i \notin \mathbb{N} \\ X_i^{k+1}(\eta_i) & for\ \eta_i \in \mathbb{R} \end{cases} \tag{35}$$

where $\mathbb{N}$, contains real positive integer members of reduce location search space.

For swarm exploration, exploitation and fast convergence, the inertia weight is defined as a function of PSO iteration number and maximum iteration [7] as expressed in Eq. (36).

$$\omega_{it} = \omega_o - 0.8 * \frac{it - 1}{Maxit - 1} \tag{36}$$

where $\omega_{it}, \omega_o, it$ and $Maxit$ are the inertia weight at a given iteration, initial weight, iteration number and maximum iteration respectively.

5.1. Algorithm for DG optimal planning to account for FACTS

- Rank lines based on severity of LVSI: Identify stressed lines and buses common to these lines at the transmission section from the results of various LVSI.
- Form reduce search space for FACTS location: First few severe lines of LVSI ranking and buses common to these severe lines constitutes reduce search space for TCSC and SVC optimal locations respectively.
- Run LVSI-PSO: Locate and size TCSC and SVC using LVSI-PSO with fitness as given in Eq. (29).
- Model Transmission section: Determine Thevenin's equivalent parameters E_{th} and Z_{th} using Eqs. (1)–(3).
- Form reduced search space for DG location: Search space for DG location and sizing constitutes all PQ nodes of distribution section.
- Locate and Size DG: Locate and size DG using PSO with fitness as given in Eq. (29).

Highlight of this paper are:

(i) Hybrid LVSI-PSO for TCSC and SVC location and sizing.
(ii) Comparison of Thevenin's equivalent and integrated transmission-distribution models with TCSC and SVC.
(iii) DG optimal planning solution accounting for TCSC and SVC with comparison of DG models.

6. Test system

Fig. 4 shows single line diagram of the test system which is an integrated transmission-distribution network. The Modified IEEE 9 bus (is the Western System Coordinating Council WSCC, network) is modelled as transmission section. The network is at 230 kV nominal voltage. It consists of 3-PQ loads, 3-transformers and 6-transmission lines. Normal total load of the IEEE 9 bus system are 315 MW and 115 MVar. The modification involves increment in reactive load demand at bus-5. Net load of the modified network are 315 MW and 235 MVar; this give rise to an increased power loss and voltage drop due to Var deficiency. Hence, the need for FACTS deployment. The distribution section is IEEE 16 nodes and 3-feeders network. There are 13 PQ nodes with net loading of 28.7 MW and 17.3 MVAR which is basically a 23 kV primary DN. From Eq. (30), DG size operational constraints is such that $P_{DG}^{max} = 22$ MW and $Q_{DG}^{max} = 13$ MVar. Test systems data are available from [46,47].

6.1. Implementation

The Open source MATLAB based load flow solver, MATPOWER is adopted to implement the solution methodology [48]. Implementation involves bidirectional data exchange between MATLAB which implement PSO and MATPOWER to evaluate static voltage stability indices and fitness function of Eq. (29). Table 1 gives PSO parameter both for FACTS and DG optimal location and sizing.

7. Results and discussion

7.1. Optimal location and size of TCSC and SVC

The proposed LVSI-PSO is applied separately with TCSC and SVC location and sizing. Table 2 shows line voltage stability indices of severe transmission lines in descending order of severity, from which reduce search space is obtained.

Figs. 5 and 6 depict typical convergence characteristics of LVSI-PSO and PSO for TCSC and SVC respectively, while optimal solutions are in Table 3. As depicted in Figs. 5 and 6, LVSI-PSO takes about ten and twenty iterations for TCSC and SVC respectively. It is also observed that LVSI-PSO provide superior minimum fitness. The low number of iterations and superior fitness value translate to reduce computational time at higher efficiency. This improved performance can be attributed to the reduce search space ability of the proposed LVSI-PSO. From Tables 3, Figs. 5 and 6, SVC with 107.929 Mvar injection at bus-5 performs better in terms of fitness

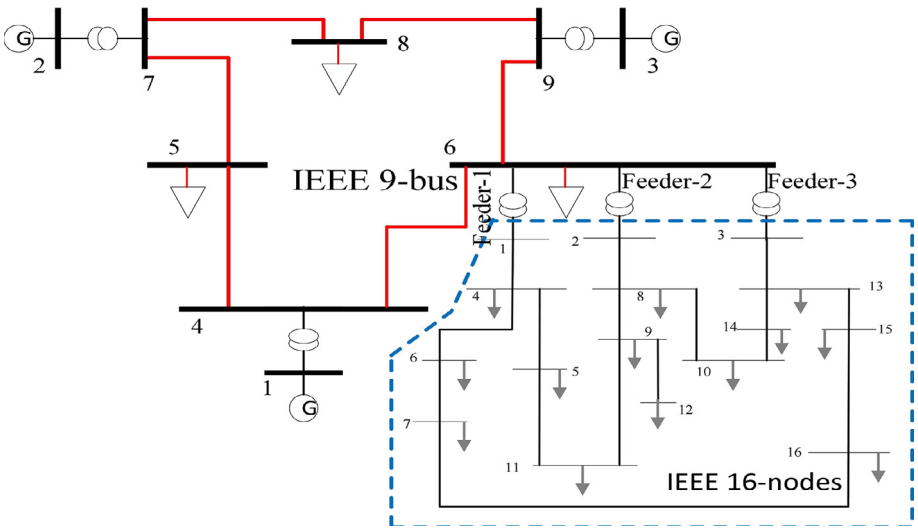

Fig. 4. Single line diagram of integrated transmission-distribution network.

Table 1
PSO parameters.

Equipment Type	ω_0	ω_{it}	C_1	C_2	Max it It	Swarm size Size
FACTS	0.9	Eq. (36)	1.5	4-C2	70	7
DG	0.9	Eq. (36)	1.5	4-C1	200	20

Table 2
LVSI with QD at bus 5 = 150 MVAR without FACTS.

From	To	L_{ij}	L_{mn}	*LQP*	*LCPI*
7	5	0.4454	0.4454	0.5462	0.6108
4	5	0.3542	0.3542	0.3498	0.3554
9	6	0.2081	0.2081	0.2358	0.2774

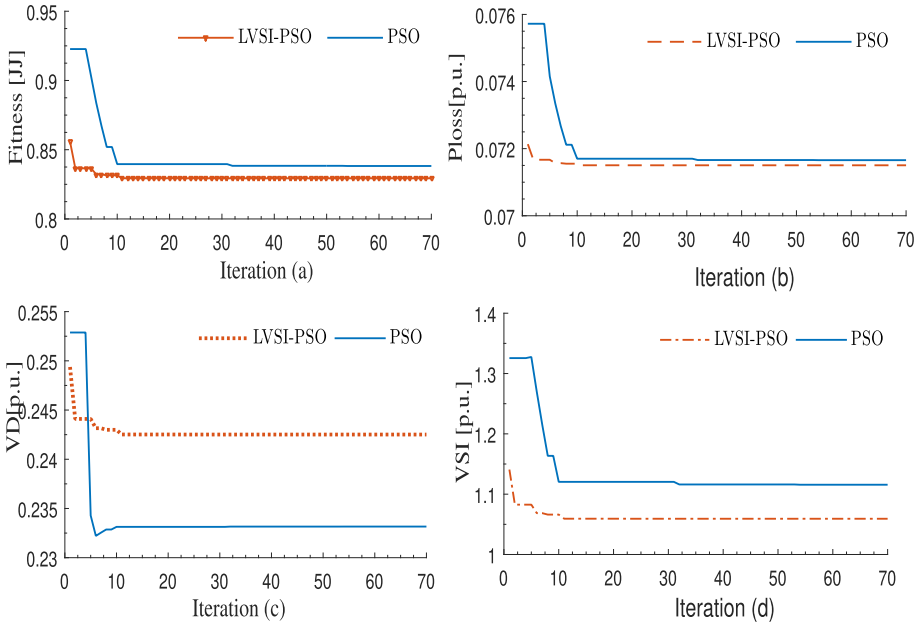

Fig. 5. Convergence characteristics of various fitness terms with TCSC.

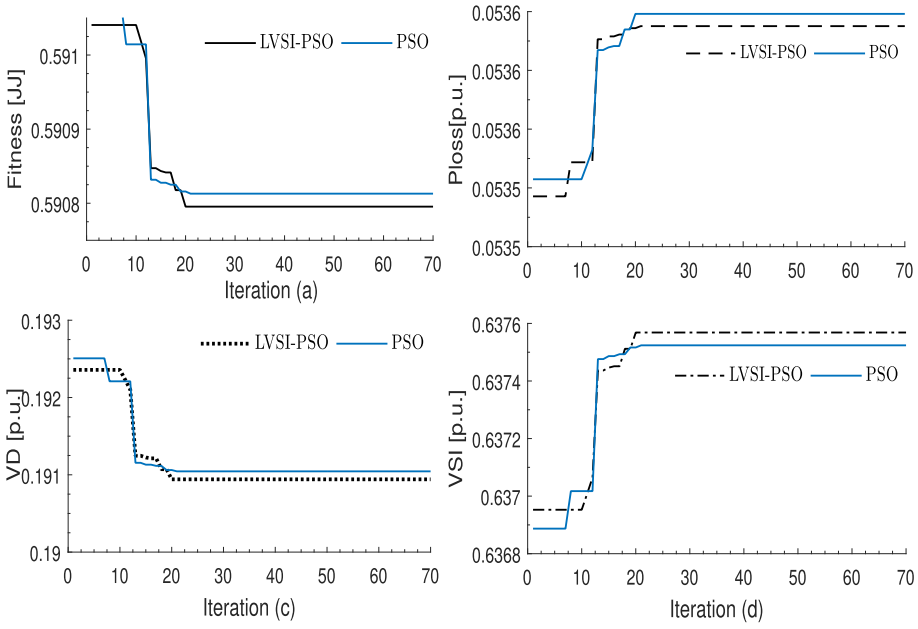

Fig. 6. Convergence characteristics of various fitness terms with SVC.

Table 3
Optimal solutions of FACTS locations and sizes.

FACTS	Loc	Size	Ploss (p.u.)	V_D (p.u.)	LVSI (p.u.)
No FACTS	–	–	0.0778	0.2842	1.5339
TCSC	line 4–5	79.98%	0.0715	0.2425	1.0593
SVC	bus 5	107.929Mvar	0.0536	0.1909	0.6375

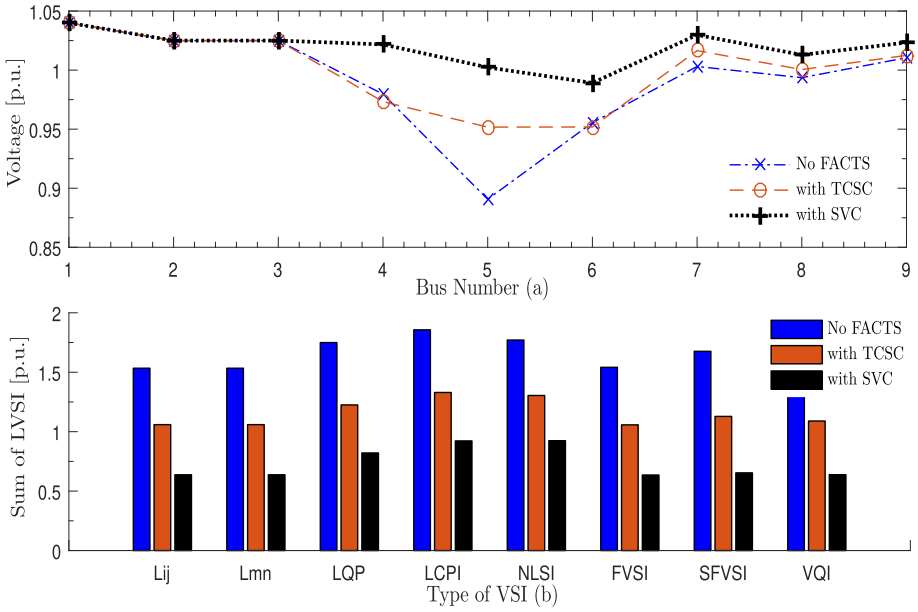

Fig. 7. (a) Voltage profile and (b) Line voltage stability indices with/without.

Table 4
Thevenin's equivalent parameters.

Thevenin's Parameters	No FACTS	With TCSC	With SVC
E_{th} (p.u.)	1.0632	1.0554	1.0822
$\phi_{th}(^\circ)$	−6.3169	−6.2883	−7.3757
Z_{th} (p.u.)	0.3016 + 0.0685i	0.2903 + 0.0615i	0.2995 + 0.0212i

function terms of Eqs. (20), (22)than TCSC with percentage compensation of 79.98% at line 4–5.

Fig. 7 shows performance in terms of voltage profile (Fig. 7(a)) and line voltage stability indices (Fig. 7(b)) with and without FACTS. This is expected as the impact of TCSC is to redistribute line power flows while SVC compensate the Var deficient test system.

Following FACTS optimal solution in Table 3, Thevenin's parameters with and without FACTS are obtained in Table 4. Impact of TCSC and SVC is observed as decrement and increment of Thevenin's voltage respectively as well as modification of Thevenin's impedances. The change in Thevenin's voltage is due to the effective net impedance of the network according to Eqs. (4) and (6) with TCSC and SVC respectively. In addition, while TCSC redistributes line power flows, SVC compensate the Var deficiency through reactive power injection. As shown in Fig. 7(a), impacts of TCSC and SVC placement modifies the network voltage profile and hence the changes in Thevenin's voltage.

7.2. Optimal DG planning

For comparison, three transmission section models were used. Initially, transmission network is represented as slack bus and modelled as 1.0p.u without substation as often documented in [15] and other literatures, second model is the integrated test system described by Fig. 4 [13]. Thirdly, the proposed model based on Thevenin's equivalent.

To validate the proposed methodology, results obtained from integrated Transmission-distribution network of Fig. 4 is considered the accurate optimal DG planning solutions, thus used as basis of comparison. Three transmission network models compared are described in detail as follows;

Model-A (Integrated test system): is 1EEE 9 bus and IEEE 16 nodes of Fig. 4. At PCC, voltage transformation is 230/23 kV. Transmission and distribution sections are at a nominal of 230 kV and 23 kV respectively.
Model-B: here, each of the three feeder nodes of the IEEE 16 nodes distribution network are modelled as PV at 1.0 pu., as reported in [15]. This is equivalent to Fig. 4 excluding transmission section. Under this model, three cases were considered due to change of slack bus as follows;
Feeder-1: Feeder 1 is taken as slack bus.
Feeder-2: Feeder 2 is taken as slack bus.
Feeder-3: Feeder 3 is taken as slack bus.
Model-C(Thevenin's equivalent): as stated earlier, this implement the proposed Thevenin's equivalent model of transmission section with FACTS, it is obtained using the Thevenin's equivalent of Fig. 4, as given in Fig. 1. DG location and size within distribution section of all models for PV and PQ types of are often grouped into three major s were considered. Three cases were simulated under **Model-A** and **Model-C** with each DG type for comparison thus;
Case-i: No FACTS for both PV and PQ type DG
Case-ii: TCSC for both PV and PQ types DG
Case-iii:SVC for both PV and PQ types DG.

Figs. 8 and 9 shows convergence characteristics of three cases of DG optimal planning solutions, with PV and PQ types of DG integration in **Model-A** respectively. From Figs. 8 and 9, PV and PQ types of DG integration with optimally placed SVC gives better performance compared with TCSC and without FACTS. In Figs. 8(b) and 9(b), impacts of line power flow redistribution by TCSC results in slight increase in power loss at distribution sections. Similar impacts are observed in terms of voltage deviations and static stability indices. This is attributable to slight decrease in voltage with TCSC at PCC (bus 6) as evident in Fig. 7(a).

In Figs. 10 and 11, convergence characteristics of all cases under **Model-B** for both PV and PQ types of DG are depicted respectively. Optimal DG solutions from **Model-B** with both PV and PQ types of DGs did not match that of **Model-A** for all cases of feeders chosen as slack. Moreover, **Model-B** cannot account for impacts of FACTS on DG integrations. Consequently, Figs. 12 and 13 depicts convergence characteristics of the proposed **Model-C** for both PV and PQ types of DG respectively.

Tables 5 and 6 show optimal DG planning solution for all models, with PV and PQ types of DG respectively. For a multi feeder IEEE 16 node distribution network with unbalance load distribution along feeders, amount of power flows through each feeder also differs. In load flow computations, in addition to being the reference node, a slack node is specified to supply network losses. As a result, choice of slack node changes the amount of power flows through each feeder. This affect DG sizes as shown in Tables 5 and 6. Also, slack node choices ensure exhaustive and realistic comparison with both **Model-A** and **Model-C** respectively.

To improve power quality indices, TCSC redistributes power flows away from heavily loaded lines. Although, the resulting effect improves voltage profile at the Var deficient bus as shown in Fig. 7 (a), it may cause additional power losses in lines with increased

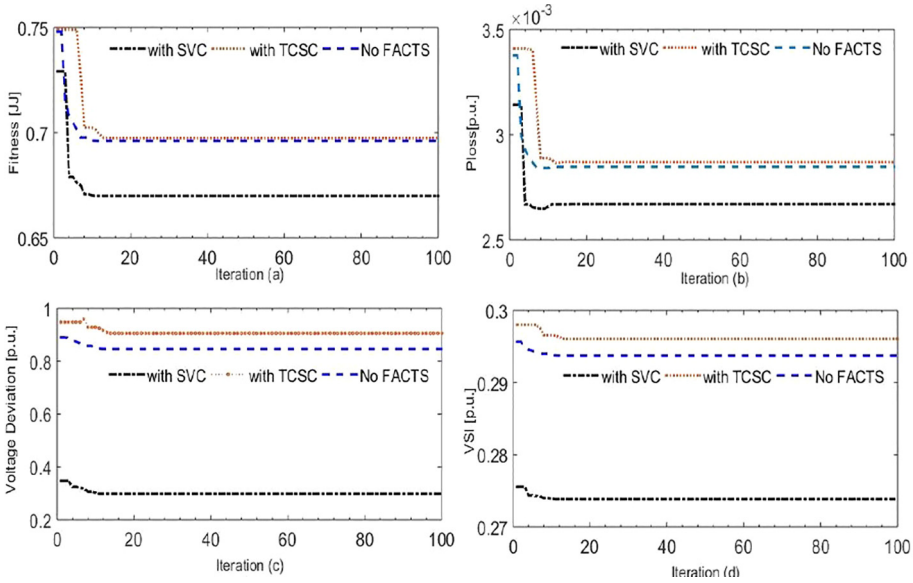

Fig. 8. Convergence characteristics of **Model-A** for PV-type DG.

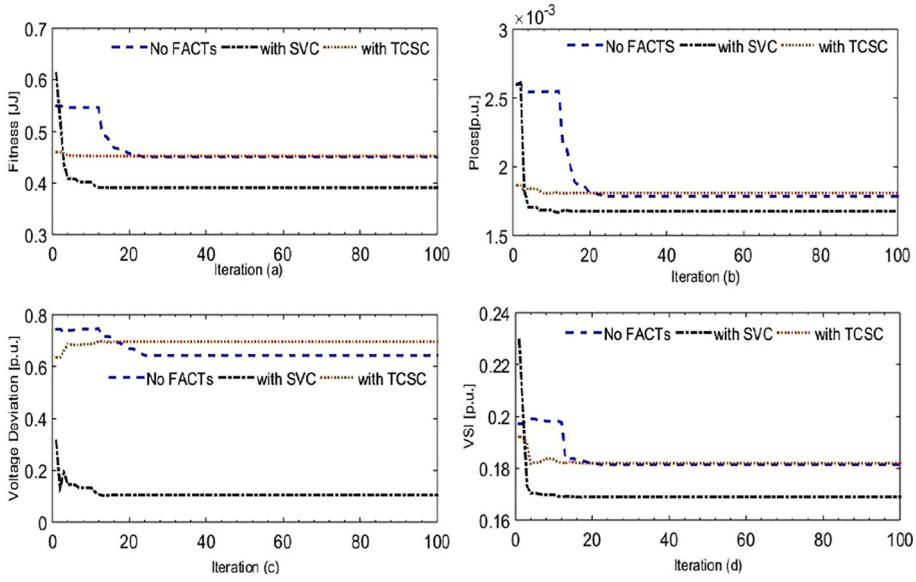

Fig. 9. Convergence characteristics of **Model-A** for PQ-type DG.

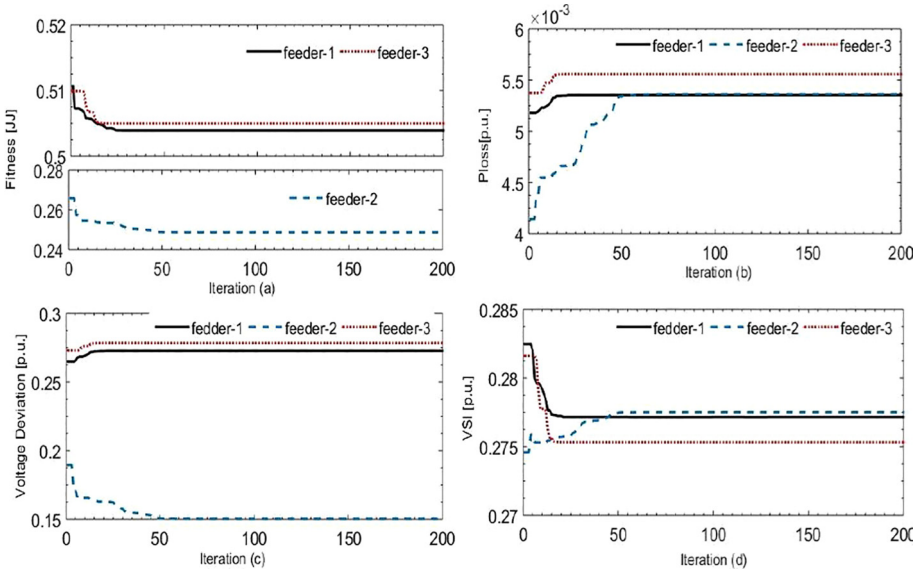

Fig. 10. Convergence characteristics of **Model-B** for PV-type DG.

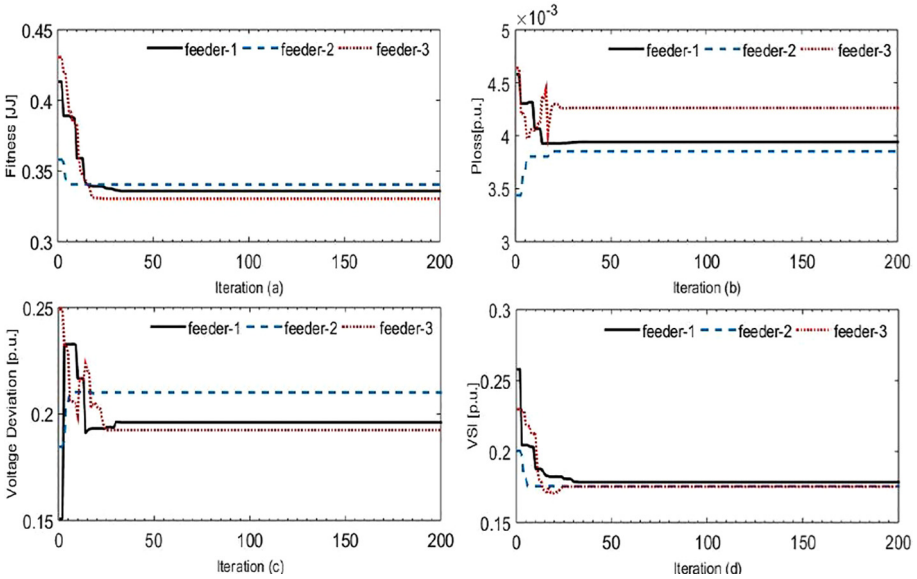

Fig. 11. Convergence characteristics of **Model-B** for PQ-type DG.

flows due to TCSC incorporation. Furthermore, fitness value in FACTS placement is a compromise between the three fitness terms (J_1,J_2 and J_3). Hence, the effects of power flow redistribution results in a slight rise in power loss and voltage deviation at distribution sections as shown in Tables 5 and 6 for **Model-A** and **Model-C**.

From Figs. 12 and 13, optimal DG planning solution with **Model-C** match that of **Model-A** and follows similar pattern where DG integrations with SVC produces better results compared with TCSC and without FACTS. Figs. 12(d) and 13(d) shows that TCSC results in a higher static line voltage stability index. Similar trend is observed in case of power loss and voltage deviation as depicted in Figs. 12(a and c) and 13(a and c); this confirm that the proposed **Model-C** emulates **Model-A**.

Radar diagram of Fig. 14 depicts improved voltage profile of distribution section with DG for all three cases using **Model-C**. It is noted that overall impacts of both SVC and TCSC at transmission section further improves voltage profile at the distribution section with DG. From Fig. 14, Tables 5 and 6, PQ type of DG with SVC results in utmost improvement in voltage profile and fitness terms in both **Model-A** and **Model-C**.

7.3. Sensitivity analysis

Contingencies in transmission section such as sudden loss of load, single line outage (N – 1), change in loading pattern and topology propagates into the distribution section. Degradation in power quality indices is the resultant effect, this also affects distribution section planning and operations.

Fig. 15 shows variation of Thevenin's voltage with V_{pcc}. For an operating voltage of $0.9 \leqslant V_{th} \leqslant 1.1pu, V_{th}$ below 0.9 pu models contingencies such as sudden increase in loads or loss of transmission lines which causes voltage dips while V_{th} above 1.1 pu models sudden loss of load and causes voltage rise both at point of common coupling.

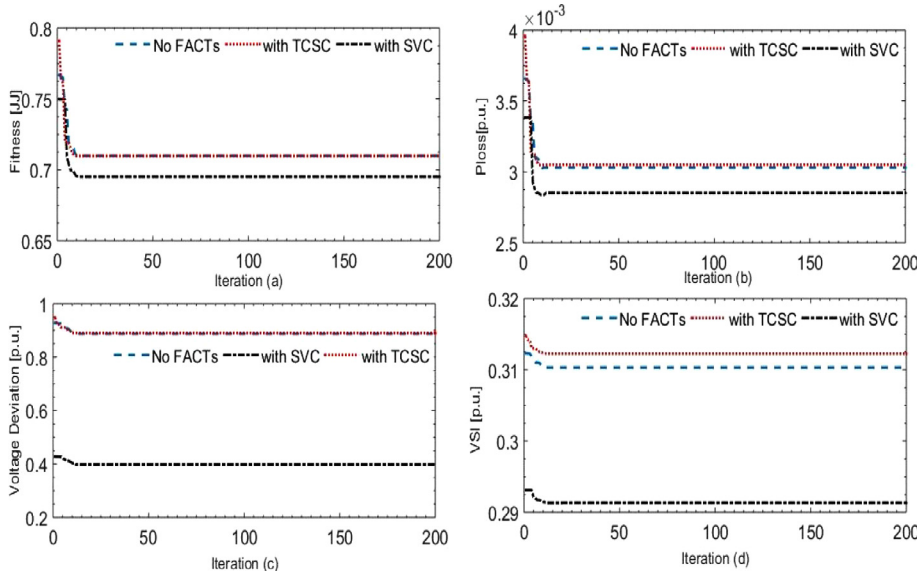

Fig. 12. Convergence characteristics of **Model-C** for PV-type DG.

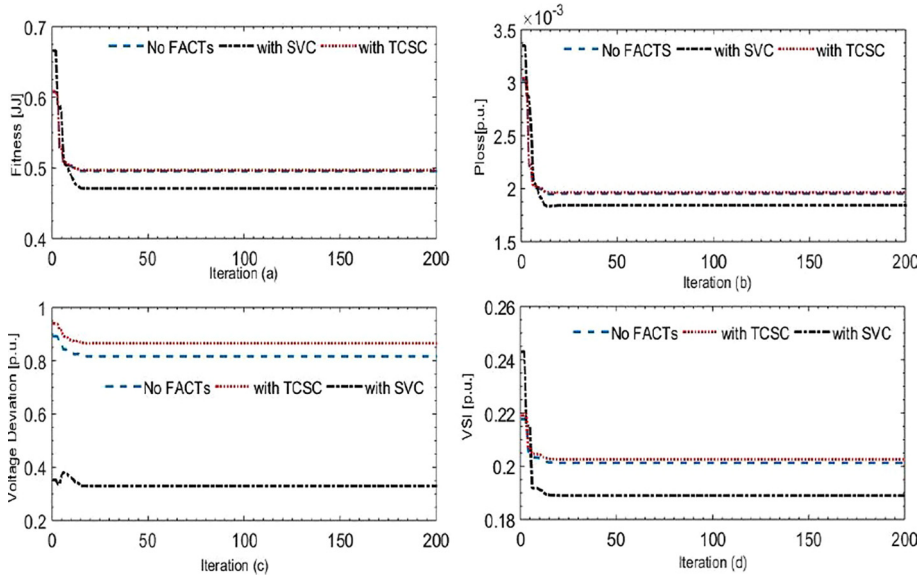

Fig. 13. Convergence characteristics of **Model-C** for PQ-type DG.

Table 5
Optimal DG planning solution of all models with PV type of DG.

	Model-A			Model-B			Model-C		
Optimal Solution	No FACTS	with TCSC	with SVC	Feeder-1 Slack	Feeder-2 Slack	Feeder-3 Slack	No FACTS	with TCSC	with SVC
V_{pcc} (p.u.)	0.955	0.951	0.988	1.0	1.0	1.0	0.957	0.954	0.989
Node	9	9	9	6	12	6,7,16	9	9	9
PVSize (MW)	17.069	17.032	17.775	1.0902	6.865	0.00214	17.277	17.256	17.7008
Ploss (p.u.)	0.00285	0.0029	0.0027	0.00535	0.00403	0.00556	0.00303	0.0031	0.00281
VD (p.u.)	0.84616	0.9062	0.2983	0.27256	0.2265	0.27843	0.88771	0.9365	0.39857
LVSI (p.u.)	0.29374	0.2961	0.2739	0.27723	0.26009	0.27532	0.31032	0.3123	0.29133

Fig. 16 depicts sensitivity of change in transmission section's operating states with optimal DG size. As earlier mentioned, variations in V_{th} models' changes in transmission section's operating states, hence can affect optimal DG planning solutions. Similarly, Fig. 17 shows variations in Vth with respect to fitness function of Eq. (29). From Figs. 16 and 17, with ideal transmission section model (V_{th} = 1.0 pu.), impacts of changes in operating conditions due to TCSC or SVC are obviously difficult to distinguish.

Table 6
Optimal DG planning solution of all models with PQ type of DG.

	Model-A			Model-B			Model-C		
Optimal Solution	No FACTS	with TCSC	with SVC	Feeder-1 Slack	Feeder-2 Slack	Feeder-3 Slack	No FACTS	with TCSC	with SVC
V_{pcc} (p.u.)	0.955	0.951	0.988	1.0	1.0	1.0	0.957	0.954	0.989
Node	9	9	9	9	9	9	9	9	9
PSize (MW)	17.2244	17.1950	17.380	1.7650	2.4019	1.0967	17.3497	17.315	17.7987
QSize (MVar)	8.92308	8.9164	9.0541	10.64461	7.26984	11.06967	8.98848	8.9887	8.99264
Ploss (p.u.)	0.00179	0.0018	0.0017	0.00417	0.00385	0.004262	0.00195	0.002	0.00184
VD (p.u.)	0.63623	0.697	0.1057	0.19392	0.21013	0.19249	0.81662	0.8653	0.32971
LVSI (p.u.)	0.18067	0.182	0.1691	0.17366	0.17553	0.17531	0.20128	0.2026	0.18897

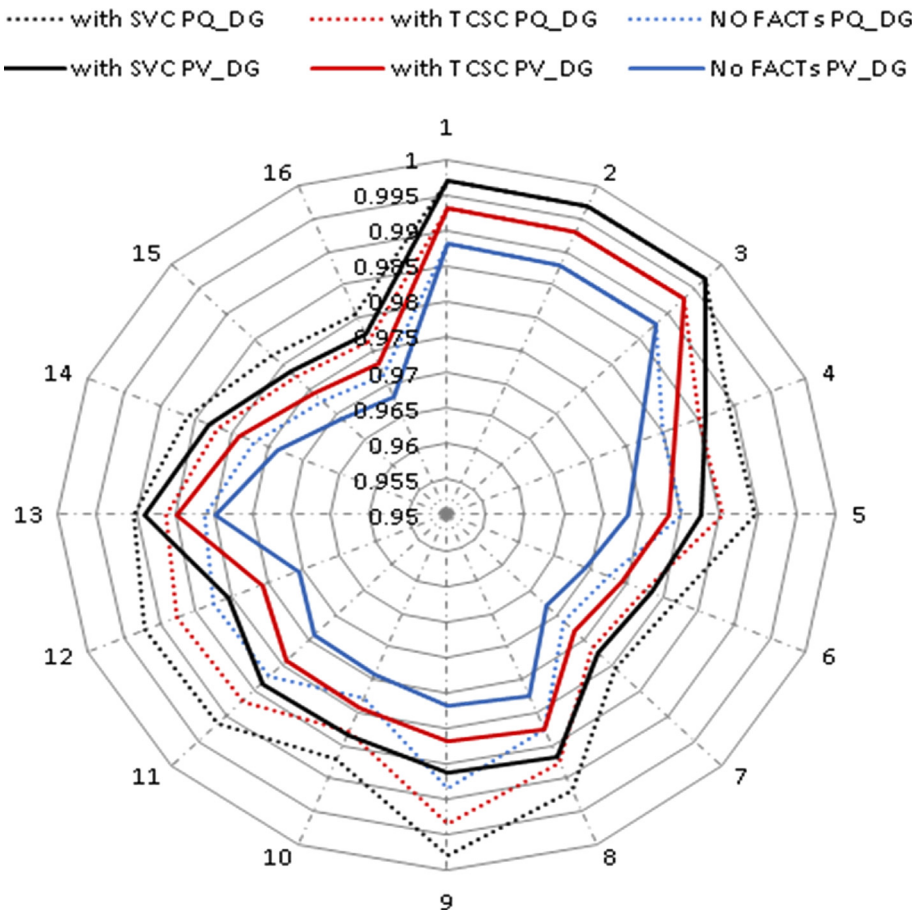

Fig. 14. Voltage profile of IEEE 16 nodes distribution network with DG.

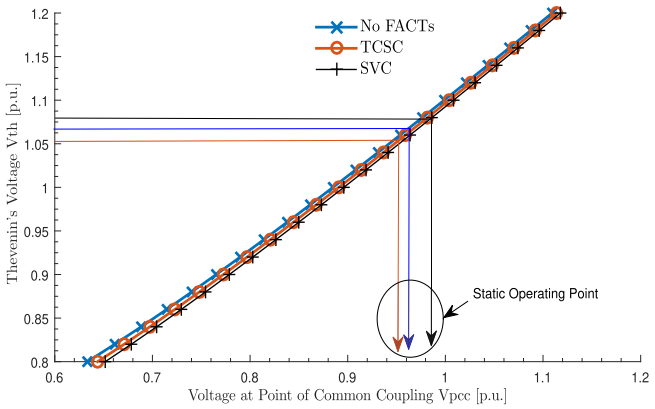

Fig. 15. Variation of Thevenin's voltage with voltage at point of common coupling.

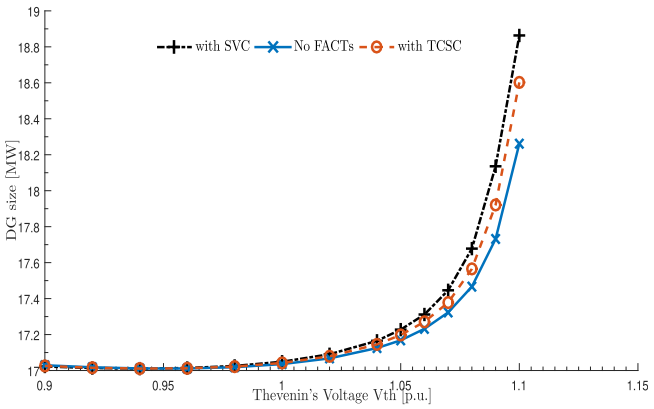

Fig. 16. Sensitivity of PV type DG sizes with Thevenin's voltage.

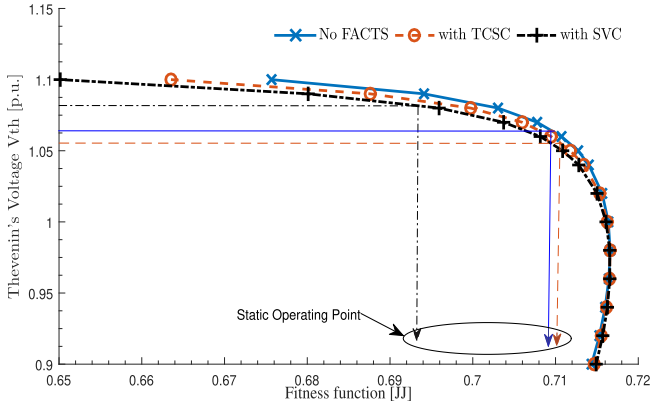

Fig. 17. Fitness function variations with Thevenin's voltage.

8. Conclusion

This paper demonstrates optimal DG planning solution in a multi-feeder (IEEE 16 node) distribution network with adequate transmission network model. Transmission section with and without FACTS is modelled by Thevenin's equivalent parameters. Results obtained are compared with an integrated transmission-distribution network with transmission section modelled by IEEE 9 bus. DG optimal planning which models Transmission section as ideal (1.0 pu.) at each feeder of a multi-feeder distribution network is inadequate and present local optimal solutions thus unable to account for impacts of FACTS. Results obtained from analysis of the test system show that, the proposed Thevenin's equivalent model is adequately able to account for the impacts of FACTS and closely matches the integrated test system. For this test system, the impacts is pronounced in optimal DG sizes. For all cases considered, PQ type of DG better improves fitness terms compared to PV type of DG, while SVC with PQ type of DG produces the utmost improved optimal solution.

References

[1] S. Ali, N. Pearsall, G. Putrus, Impact of high penetration level of grid-connected photovoltaic systems on the UK low voltage distribution network, in: Int. Conf. Renew. Energies Power Qual., Santiago de Compostella (Spain), 2012, pp. 2–5. http://www.icrepq.com/icrepq'12/368-ali.pdf.

[2] A. Ogunjuyigbe, T. Ayodele, O. Akinola, Impact of distributed generators on the power loss and voltage profile of sub-transmission network, J. Electr. Syst. Inf. Technol. 3 (1) (2016) 94–107, https://doi.org/10.1016/j.jesit.2015.11.010.

[3] S. Dahal, H. Salehfar, Impact of distributed generators in the power loss and voltage profile of three phase unbalanced distribution network, Int. J. Electr. Power Energy Syst. 77 (2016) 256–262, https://doi.org/10.1016/j.ijepes.2015.11.038.

[4] M. Jamil, A.S. Anees, Optimal sizing and location of SPV (solar photovoltaic) based MLDG (multiple location distributed generator) in distribution system for loss reduction, voltage profile improvement with economical benefits, Energy 103 (2016) 231–239, https://doi.org/10.1016/j.energy.2016.02.095.

[5] L. Mokgonyana, J. Zhang, L. Zhang, X. Xia, Coordinated two-stage volt/var management in distribution networks, Electr. Power Syst. Res. 141 (2016) 157–164, https://doi.org/10.1016/j.epsr.2016.07.012.

[6] R.M. Idris, A. Kharuddin, M.W. Mustafa, A. Khairuddin, M.W. Mustafa, A. Kharuddin, M.W. Mustafa, Optimal Allocation of FACTS devices for ATC enhancement using Bees Algorithm, Power Eng. Conf. 2009. AUPEC 2009. Australas. Univ. 3 (6) (2009) 1–6.

[7] R. Sripriya, R. Neela, SVC placement for ATC enhancement using WIPSO technique, Glob. J. Pure Appl. Math. 12 (1) (2016) 747–760.

[8] F. Khandani, S. Soleymani, B. Mozafari, Optimal allocation of SVC to enhance total transfer capability using hybrid genetics algorithm and sequential quadratic programming, in: ECTI-CON 2011-8th Electr. Eng. Electron. Comput. Telecommun. Inf. Technol. Assoc. Thail. - Conf. 2011, Thailand, 2011, pp. 861–864. doi:10.1109/ECTICON.2011.5947976.

[9] A.A. Sadiq, M.N. Nwohu, Evaluation of inter area available transfer capability of Nigeria 330KV network, Int. J. Eng. Technol. 3 (2) (2013) 148–158.

[10] C. Gaunt, E. Namanya, R. Herman, Voltage modelling of LV feeders with dispersed generation: limits of penetration of randomly connected photovoltaic generation, Electr. Power Syst. Res. 143 (2017) 1–6, https://doi.org/10.1016/j.epsr.2016.08.042. URL:http://linkinghub.elsevier.com/retrieve/pii/S0378779616303467.

[11] C.T. Gaunt, R. Herman, E. Namanya, M.J. Chihota, Voltage modelling of LV feeders with dispersed generation: Probabilistic analytical approach using beta PDF, Electr. Power Syst. Res. 143 (2017) 25–31, https://doi.org/10.1016/j.epsr.2016.09.016.

[12] C. Ma, P. Kaufmann, J.C. Töbermann, M. Braun, Optimal generation dispatch of distributed generators considering fair contribution to grid voltage control, Renew. Energy 87 (2016) 946–953, https://doi.org/10.1016/j.renene.2015.07.083.

[13] H. Jain, K. Rahimi, A. Tbaileh, R.P. Broadwater, Akshay Kumar Jain, M. Dilek, Integrated transmission & distribution system modeling and analysis: need & advantages, in: 2016 IEEE Power Energy Soc. Gen. Meet., IEEE, Boston, MA, USA, 2016, pp. 1–5, https://doi.org/10.1109/PESGM.2016.7741235. URL:http://ieeexplore.ieee.org/document/7741235/.

[14] M. Sankaramoorthy, M. Veluchamy, A hybrid MACO and BFOA algorithm for power loss minimization and total cost reduction in distribution systems, Turkish J. Electr. Eng. Comput. Sci. 25 (2017) 337–351, https://doi.org/10.3906/elk-1410-191. URL: http://online.journals.tubitak.gov.tr/openDoiPdf.htm?mKodu=elk-1410-191.

[15] D. Pandey, J.S. Bhadoriya, Optimal placement & sizing of distributed generation (DG) to minimize active power loss using particle swarm optimization (PSO), Int. J. Sci. Technol. Res. 3 (7) (2014) 246–254.

[16] S. Kabir, O. Krause, S. Bartlett, Impact of large-scale photovoltaic system on short and long term voltage stability in sub transmission networl, Australas. Univ. Power Eng. Conf. AUPEC (October) (2013) 1–6.

[17] H. Musa, B. Usman, S.S. Adamu, Improvement of voltage stability index using distributed generation for Northern Nigeria sub-transmission region, Int. Conf. Comput. Electr. Electron. Eng. Improv. (2013) 410–412.

[18] B. Fani, H. Bisheh, A. Karami-horestani, An offline penetration-free protection scheme for PV-dominated distribution systems, Electr. Power Syst. Res. 157 (2018) 1–9, https://doi.org/10.1016/j.epsr.2017.11.020.

[19] M. Armendáriz, K. Paridari, E. Wallin, L. Nordström, Comparative study of optimal controller placement considering uncertainty in PV growth and distribution grid expansion, Electr. Power Syst. Res. 155 (2018) 48–57, https://doi.org/10.1016/j.epsr.2017.10.001.

[20] R. Arulraj, N. Kumarappan, Optimal economic-driven planning of multiple DG and capacitor in distribution network considering different compensation coefficients in feeder's failure rate evaluation, Eng. Sci. Technol. Int. J. 22 (1) (2019) 67–77.

[21] G.H. Reddy, A.K. Goswami, N.B.D. Choudhury, Engineering science and technology, an international journal impact of plug-in electric vehicles and distributed generation on reliability of distribution systems, Eng. Sci. Technol. Int. J. 21 (1) (2018) 50–59, https://doi.org/10.1016/j.jestch.2018.01.005.

[22] P. Salyani, J. Salehi, F.S. Gazijahani, Chance constrained simultaneous optimization of substations, feeders, renewable and non-renewable distributed generations in distribution network, Electr. Power Syst. Res. 158 (2018) 56–69, https://doi.org/10.1016/j.epsr.2017.12.032.

[23] Y. Zhang, Y. Xu, H. Yang, Z. Yang, Voltage regulation-oriented co-planning of distributed generation and battery storage in active distribution networks, Electr. Power Energy Syst. 105 (2019) 79–88, https://doi.org/10.1016/j.ijepes.2018.07.036.

[24] F. Meng, B. Chowdhury, M.S. Hossan, Optimal integration of DER and SST in active distribution networks, Electr. Power Energy Syst. 104 (2019) 626–634, https://doi.org/10.1016/j.ijepes.2018.07.035.

[25] M. Yarahmadi, M.R. Shakarami, An analytical and probabilistic method to determine wind distributed generators penetration for distribution networks based on time-dependent loads, Electr. Power Energy Syst. 103 (May) (2018) 404–413, https://doi.org/10.1016/j.ijepes.2018.06.025.

[26] S. Gholami, S. Saha, M. Aldeen, Robust multiobjective control method for power sharing among distributed energy resources in islanded microgrids with unbalanced and nonlinear loads, Int. J. Electr. Power Energy Syst. 94 (2018) 321–338, https://doi.org/10.1016/j.ijepes.2017.07.012.

[27] K. Khalid, S. Ullah, S.-J. Lee, Z. Maqsood, M. Kashif, C.-H. Kim, A real-time optimal coordination scheme for the voltage regulation of a distribution network including an OLTC, capacitor banks, and multiple distributed energy resources, Int. J. Electr. Power Energy Syst. 94 (2018) 1–14, https://doi.org/10.1016/j.ijepes.2017.06.024.

[28] M. Haque, A fast method for determining the voltage stability limit of a power system, Electr. Power Syst. Res. 32 (1) (1995) 35–43, https://doi.org/10.1016/0378-7796(94)00893-9. URL:http://www.sciencedirect.com/science/article/pii/0378779694008939.

[29] M. Haque, Novel method of assessing voltage stability of a power system using stability boundary in PQ plane, Electr. Power Syst. Res. 64 (1) (2003) 35–40, https://doi.org/10.1016/S0378-7796(02)00117-7. URL:http://linkinghub.elsevier.com/retrieve/pii/S0378779602001177.

[30] R.J.R. Kumar, P.N. Rao, Z bus computation for networks having mutually coupled elements using uncoupled equivalents of coupled groups, in: 2014 Eighteenth Natl. Power Syst. Conf., IEEE, GUWAHATI, 2014, pp. 1–4, https://doi.org/10.1109/NPSC.2014.7103827.

[31] T. Nireekshana, G.R. Kesava, S. Sivanaga, Enhancement of ATC with FACTS devices using real-code genetic algorithm, Int. J. Electr. Power Energy Syst. 43 (1) (2012) 1276–1284, https://doi.org/10.1016/j.ijepes.2012.06.041.

[32] N.B. Choudhury, R. Jena, Available Transfer Capability enhancement in constrained network conditions using TCSC, 2014 Int. Conf. Adv. Eng. Technol. Res. ICAETR 2014. doi:10.1109/ICAETR.2014.7012804.

[33] N. Sinha, S. Karan, S.K. Singh, Modified de based ATC enhancement using FACTS devices, in: Proc. – 1st Int. Conf. Comput. Intell. Networks, CINE 2015, 2015, pp. 3–8. doi:10.1109/CINE.2015.11.
[34] T. Nireekshana, G.R. Kesava, S. Sivanaga, Available transfer capability enhancement with FACTS using Cat Swarm Optimization, Ain Shams Eng. J. 7 (1) (2016) 159–167, https://doi.org/10.1016/j.asej.2015.11.011.
[35] P. Prabhakar, A. Kumar, Voltage stability boundary and margin enhancement with FACTS and HVDC, Int. J. Electr. Power Energy Syst. 82 (2016) 429–438, https://doi.org/10.1016/j.ijepes.2016.03.038.
[36] B. Mahdad, K. Srairi, Adaptive differential search algorithm for optimal location of distributed generation in the presence of SVC for power loss reduction in distribution system, Eng. Sci. Technol. Int. J. 19 (3) (2016) 1266–1282, https://doi.org/10.1016/j.jestch.2016.03.002.
[37] S. Jahan, A.M. Mannan, Voltage stability analysis of a 16-bus distribution network based on voltage, Int. J. Multidiscip. Sci. Eng. 5 (4) (2014) 1–5.
[38] N.S. Vadivoo, S.M.R. Slochanal, Distribution system restoration using genetic algorithm with distributed generation, Mod. Appl. Sci. 3 (4) (2009) 98–110, https://doi.org/10.5539/mas.v3n4p98. URL:http://www.ccsenet.org/journal/index.php/mas/article/view/1258.
[39] N.G.A. Hemdan, M. Kurrat, Efficient integration of distributed generation for meeting the increased load demand, Int. J. Electr. Power Energy Syst. 33 (9) (2011) 1572–1583, https://doi.org/10.1016/j.ijepes.2011.06.032.
[40] M. Venkateswara Rao, S. Sivanagaraju, C.V. Suresh, Available transfer capability evaluation and enhancement using various FACTS controllers: Special focus on system security, Ain Shams Eng. J. Prod. hosting bt Elsevier 7 (1) (2016) 191–207. doi:10.1016/j.asej.2015.11.006. URL:http://linkinghub.elsevier.com/retrieve/pii/S2090447915001835.
[41] J. Modarresi, E. Gholipour, A. Khodabakhshian, A comprehensive review of the voltage stability indices, Renew. Sustain. Energy Rev. 63 (2016) 1–12, https://doi.org/10.1016/j.rser.2016.05.010.
[42] A.A. Hassan, F.H. Fahmy, A.E.-s. A. Nafeh, M.A. Abu, Genetic single objective optimisation for sizing and allocation of renewable DG systems, Int. J. Sustain. Energy 6451 (2015) 0–18, https://doi.org/10.1080/14786451.2015.1053393.
[43] E.S. Ali, S.M.A. Elazim, A.Y. Abdelaziz, Ant Lion Optimization Algorithm for optimal location and sizing of renewable distributed generations, Renew. Energy 101 (2017) 1311–1324, https://doi.org/10.1016/j.renene.2016.09.023.
[44] S.A. Chithradevi, L. Lakshminarasimman, R. Balamurugan, Stud Krill herd Algorithm for multiple DG placement and sizing in a radial distribution system, Eng. Sci. Technol. Int. J. 20 (2) (2017) 748–759, https://doi.org/10.1016/j.jestch.2016.11.009.
[45] B.M. Dennis, The Engineering Design of Systems: Models and Methods, second ed., John Wiley & Sons, New Jersy, 2009.
[46] P. Subburaj, K. Ramar, L. Ganesan, P. Venkatesh, Distribution system reconfiguration for loss reduction using genetic algorithm, J. Electr. Syst. 2 (4) (2006) 198–207.
[47] A.S. Ahmad, Inter-Area Transfer capability Assessment of Nigerian 330KV Network (Tech. rep.), Federal University of Technology, Minna. Nigeria, 2013. URL:http://dnb.d-nb.de.
[48] R.D. Zimmerman, C.E. Murillo-Sanchez, R.J. Thomas, MATPOWER: steady-state operations, planning, and analysis tools for power systems research and education, IEEE Trans. Power Syst. 26 (1) (2011) 12–19, https://doi.org/10.1109/TPWRS.2010.2051168. URL:http://ieeexplore.ieee.org/lpdocs/epic03/wrapper.htm?arnumber=5491276.